Ab initio Bethe-Salpeter calculations of the x-ray absorption spectra of transition metals at the *L*-shell edges

J. Vinson and J. J. Rehr
Department of Physics, University of Washington, Seattle, Washington 98195, USA
(Received 18 May 2012; published 26 November 2012)

We present *ab initio* Bethe-Salpeter equation (BSE) calculations of the $L_{2,3}$ edges of several insulating and metallic compounds containing Ca, V, Fe, Co, Ni, and Cu, spanning a range of $3d$-electron occupations. Our approach includes the key ingredients of a unified treatment of both extended states and atomic multiplet effects, i.e., Bloch states, self-consistent crystal potentials, ground-state magnetism, GW self-energy corrections, spin-orbit terms, and Coulomb interactions between the L_2 and L_3 levels. The method is implemented in the OCEAN package, which uses plane-wave pseudopotential wave functions as a basis, a projector-augmented-wave construction for the transition matrix elements, and a resolvent formalism for the BSE calculation. The results are in near quantitative agreement with experiment, including both fine structure at the edges and the nonstatistical L_3/L_2 ratios observed for these systems. Approximations such as time-dependent density-functional theory are shown to be less accurate.

DOI: 10.1103/PhysRevB.86.195135 PACS number(s): 78.70.Dm, 71.15.Qe, 78.20.Bh

I. INTRODUCTION

X-ray-absorption spectra (XAS) at the $L_{2,3}$ edges of $3d$ transition-metals are dominated by spin-orbit (SO) split "white lines," i.e., transitions from the occupied $2p_{1/2}$-$2p_{3/2}$ core states to unoccupied, quasilocalized $3d$ states. Strikingly, their L_3/L_2 white-line intensity ratios deviate from the statistical 2:1 value, ranging from 0.8 to above 2.0 with increasing atomic number.[1] Despite many attempts and a variety of theoretical frameworks including atomic multiplets,[2,3] configuration interaction,[4,5] time-dependent density-functional theory (TDDFT),[6–8] multichannel multiple scattering,[9,10] and Bethe-Salpeter equation (BSE) based approaches,[11,12] none has heretofore quantitatively accounted for the variation in the L_3/L_2 ratio and extended fine structure for both metallic and insulating compounds across the range of d-band occupations. Needed is a first-principles theory that unifies the local atomic multiplet approach with extended states, taking into account the dominant atomic (spin orbit, intra-atomic couplings, and lifetime effects for multiple core levels) and solid-state effects (spin-dependent potentials, quasiparticle shifts, and lifetimes), as well as the interactions between them.

To address this need, we present a GW BSE approach based on many-body perturbation theory (MBPT) for calculating the core-level L-edge spectra of materials with $3d$ elements which builds in all of these effects. The method is implemented as an extension of the recently developed OCEAN package,[13] which utilizes pseudopotential based wave functions, e.g., from the ABINIT electronic-structure package,[14,15] the core-level BSE solver of Shirley,[16] and a model GW self-energy, as described below. Our implementation is applicable to both metallic and insulating compounds, contains no fitting parameters, and scales well up to unit cells of moderate size ($\approx$500 Å^3 or 200 valence electrons).[17] An early version of this approach was shown to give good results for transition-metals in a d_0 ground-state configuration, namely, Ca^{2+} and Ti^{4+}, including multiplet structures.[13,16] Unique in our present treatment is the inclusion of broadening from both core-hole lifetimes together with a complex electron self-energy, effects that were ignored in previous BSE calculations.[11] We obtain near quantitative results for the $L_{2,3}$ edges of several $3d$ transition-metal materials, covering a range of $3d$ occupancies. In contrast, we find that approximations such as TDDFT can be significantly less accurate. In the remainder of this paper, we present in Sec. II an overview of the theory and key approximations, followed in Sec. III by a number illustrative calculations and comparisons to experiment and other theoretical approximations, and we conclude in Sec. IV with a summary and suggestions for future developments.

II. THEORY

Calculations of excited-state phenomena such as dielectric response and core-level x-ray-absorption spectra (XAS) generally require techniques beyond the independent-particle approximation. Thus DFT alone or improvements such as TDDFT are often inadequate. The case of L-shell spectra of transition-metal materials, where both local atomic and long-range solid-state effects contribute, provides a severe test of the theory. Here we focus on a MBPT approach in which the Kohn-Sham DFT orbitals are replaced with quasiparticle states that include the GW self-energy of Hedin, and the excitation energies are calculated using the Bethe-Salpeter Equation (BSE). Here G is the electron Green's function and W is the screened Coulomb interaction. Such GW corrections have been remarkably successful in calculating band gaps in insulators as well as conduction and valence-band widths and inelastic losses. In addition, electron-hole spectroscopies such as XAS require particle-hole interactions that include an accurate treatment of the screened core-hole potential and electron-hole dynamics. This is carried out here for core excitations using a resolvent-based BSE approach:[16]

$$\mu(\omega,\mathbf{q}) \propto \langle 0|D^\dagger[\omega - H_{\rm BSE}]^{-1}D|0\rangle, \qquad (1)$$

where $D = \sum_{ij} c_i^\dagger c_j \langle i|d|j\rangle$ represents the interaction with an x ray which excites an electron from core level j to conduction level i, and $\langle i|d|j\rangle$ is the (e.g., dipole) transition matrix element. The BSE Hamiltonian $H_{\rm BSE}$ includes independent-particle terms for the photoelectron H_e and core hole H_h, as

well as interaction terms $H_{\rm eh}$:

$$H_{\rm BSE} = H_e - H_h + H_{\rm eh}. \quad (2)$$

As noted by Shirley,[16] the ingredients in $H_{\rm BSE}$ are similar to those used in ligand field multiplet calculations;[2] however, the BSE uses a single Slater determinant with higher-order terms embedded in screening corrections. Here,

$$H_{\rm eh} = V_X - W \quad (3)$$

corresponds to keeping only the lowest-order interactions in the BSE: the exchange and direct, respectively. This is equivalent to using the GW approximation for the self-energy when constructing the BSE kernel.

The photoelectron contribution H_e is calculated starting from DFT within either the local-density approximation (LDA) or local spin-density approximation (LSDA); H_e also includes a complex self-energy $\Sigma(E)$, which is approximated as a function of only the quasiparticle energy E:

$$H_e = E_{n,\mathbf{k},\sigma} + \Sigma_{n,\mathbf{k},\sigma} \approx E_{n,\mathbf{k},\sigma} + \Sigma(E), \quad (4)$$

where n,$\mathbf{k}$, and σ represent the band index, Bloch vector, and spin, respectively. Spin-orbit (SO) effects on the valence- and conduction-band states ($3d$, $4d$, etc.), are neglected for the materials studied, since they are much smaller than lifetime broadening effects; however, magnetic splitting is allowed for the heavier $3d$ metals. Quasiparticle corrections, including energy shifts and lifetime broadening, are incorporated using two alternative approaches within Hedin's GW approximation for the self-energy $\Sigma = iGW$, where $W = \epsilon^{-1}v$ is the screened Coulomb interaction, v the bare interaction, and ϵ the dielectric matrix. Our main approximation for Σ is the many-pole self-energy (MPSE),[18] leading to energy dependent stretching and damping of the spectra. The MPSE is based on a zero-momentum representation of the loss function $-\mathrm{Im}\,\epsilon^{-1}(\omega,\mathbf{q}\to 0)$ as a reasonably dense series of poles, making the self-energy calculation very efficient. The loss function is calculated using a companion *ab initio* valence GW BSE package AI2NBSE.[19] The MPSE can fail when the Kohn-Sham orbitals are not good approximations to the quasiparticle wave functions, in which case a self-consistent, iterative GW method is called for. For example, the low-temperature insulating phase of VO_2 is ungapped for both DFT and single-shot GW calculations, while self-consistent GW (SCGW) calculations give improved results for the ground-state properties, as will be discussed in the results section.

The hole Hamiltonian $H_h = \epsilon_j + \chi_J - i\Gamma_J$ includes a SO term χ_J and lifetime broadening Γ_J for each core level j, both of which depend on the projection of the total angular momentum J. The absolute $2p$ core-level binding energies ϵ_j and lifetime broadenings Γ_J are determined by experiment, not calculated. In this work the core wave functions and unscreened core-hole potentials are calculated within an atomic, scalar-relativistic DFT framework. Furthermore, a localized basis based on the projector-augmented-wave formalism[20] is constructed for calculating both the matrix elements D and evaluating the short-ranged parts of the electron-hole interaction $H_{\rm eh}$. Taking advantage of the local nature of the core-hole wave function, the interaction terms can be expanded in spherical harmonics and expressed as $H_{\rm eh} = V_j + g(\alpha,\beta)$. This includes the screened core-hole interaction V_j which is diagonal in the core-hole states j and Coulomb integrals $g(\alpha,\beta)$ which lead to scattering between electron-hole pairs α and β and can be recognized as the Slater integrals F^k and G^k. The form of $H_{\rm eh}$ is crucial for quantitative agreement between experiment and theory. Thus approximations such as TDDFT, where the nonlocal part of $H_{\rm eh}$ is replaced by an exchange-correlation kernel f_{xc}, are at best only semiquantitative, as discussed further below.

The direct term is attractive and reduces the excitation energies compared to the noninteracting limit, while the exchange term increases them. The exchange interaction mixes both electron and hole states, leading to variations in the crystal-field split d states and L_3/L_2 ratio, respectively. Details of the core mixing depend primarily on the atomic $2p$ core states, so the L_3/L_2 ratio is only weakly dependent on the solid-state environment. The lack of multiconfigurations in the atomic calculations leads to an overestimate of the exchange integrals, which is corrected by scaling by an *ad hoc* factor of 0.85 for all the $3d$ transition-metal $L_{2,3}$ edges, as in Ref. 2. The direct term is screened by the electronic environment and varies dramatically between insulators and metallic systems. In general the screening is a function of both frequency and momentum, but for the near edge (well below the onset of plasmon excitations, typically around 10–20 eV) it can be approximated as static, with dynamic effects neglected. For systems with strong, low-energy excitations, however, this static approximation is not valid. Here the screening is calculated numerically in real space using the random-phase approximation (RPA) within a radius of 8 bohrs around the core-hole site, while a model dielectric function is used beyond.[12,21] The screening is only calculated for the spherical direct term F^0; because higher-order terms are more localized, their screening is assumed to be slight and approximated by scaling, as for the exchange term.

For comparison we have also carried out calculations using two alternate treatments of the electron-hole interaction: the random-phase approximation (RPA) and TDDFT. The RPA neglects the direct term W in the BSE Hamiltonian while keeping only the exchange V_X. In TDDFT the direct term W is replaced by an exchange-correlation kernel $H_{\rm eh} = V_X - f_{xc}$. Here we use the adiabatic time-dependent-LDA (TDLDA) $f_{xc}(\mathbf{r},\mathbf{r}',\omega) = \delta(\mathbf{r}-\mathbf{r}')\delta v_{xc}[\rho(\mathbf{r})]/\delta r$. The density is the all-electron density of the ground-state system. The computational advantage of TDLDA is that the interaction is local and thereby efficient to calculate. Further, we constrain the TDLDA kernel to be spherical, yielding identical selection rules as the exchange interaction. The inclusion of the TDLDA therefore only provides a reduction of the exchange interaction, albeit one that is system dependent by way of the ground-state density.

III. RESULTS

All calculations were carried out using experimental lattice parameters. Gaussian broadening was added to match experimental broadening effects, supplementing the previously mentioned lifetime broadening from the photoelectron (Σ) and core hole (Γ). Also the theoretical spectra are shifted to align with experiment. Pseudopotentials for the transition-metals were constructed using the OPIUM package,[22] including the

$3s$ and $3p$ states as valence. This has been shown to increase fidelity of the pseudopotential's scattering properties at higher energies.[23] Other sources of broadening, such as phonon coupling[24] and multielectron satellites, can have noticeable effects on measured spectra, but such dynamic screening effects are currently neglected. Our results are summarized below.

A. Ca and CaF_2

Both metallic Ca and CaF_2 exhibit small splittings in the unoccupied d states, but in the metallic case this is hidden by final-state broadening of the photoelectron. The effective $2p$ SO splitting is reduced by the exchange interaction but still slightly overestimated, as in previous BSE calculations.[11,16] This overestimate is consistent for both materials, pointing to discrepancies in the atomic treatment rather than a failure of the DFT approximation for the wave functions for the valence and conduction bands. Overall the agreement of the BSE calculations with experiment is very good and gives accurate L_3/L_2 ratios for both Ca (Fig. 1) and CaF_2 (Fig. 2).

For both systems we also calculated the $L_{2,3}$ edges within the TDLDA. These TDLDA results agree well with the recent survey by Bunău and Joly.[8] As can be seen for both the metallic (Fig. 1) and insulating systems (Fig. 2), TDLDA fails to reproduce quantitatively the shape of the edge; this is due to excitonic binding which even in metallic systems can be strong for localized states, e.g., the $3d$. As remarked earlier, the spherical TDLDA kernel implemented here obeys the same selection rules as the exchange interaction but enters with opposite sign. In the Ca $L_{2,3}$ edge this can be seen by noting the TDLDA result is between the RPA and noninteracting LDA.

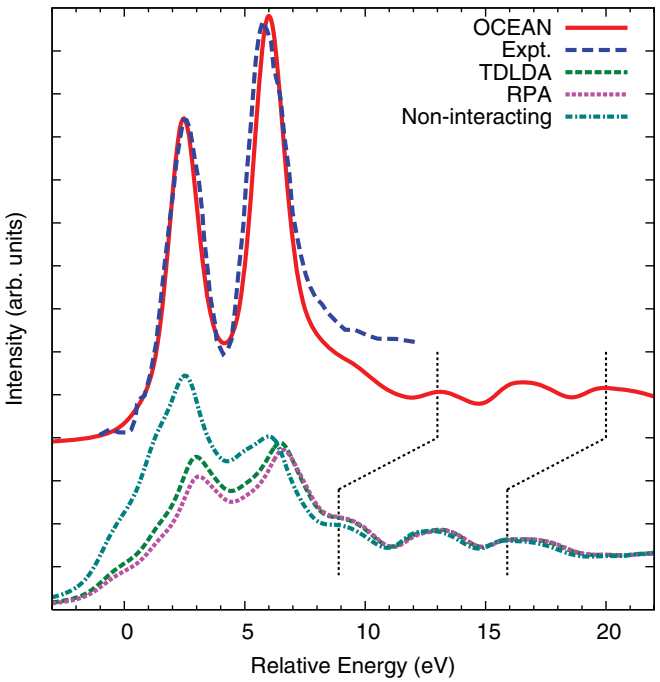

FIG. 1. (Color online) Calculated $L_{2,3}$ edge of metallic Ca compared to experiment.[25] Upper curves: The experiment scaled and aligned to match the BSE calculation at the L_3 edge. Lower curves: Several theoretical approximations shown for comparison and offset vertically for clarity: noninteracting, RPA, and TDLDA. While both the TDLDA and the RPA show reweighting of the L_3/L_2 edges from the noninteracting LDA result, the structure of the edge is still much too broad compared with experiment, retaining its independent-particle character. Due to excitonic binding, the BSE results have been shifted up by 4.1 eV with respect to the other theory curves, which are aligned at $E_F = 0$. The dotted black lines show how the delocalized postedge features are unaffected by the screened core-hole potential, which without the shift would be nearly the same in all four calculations.

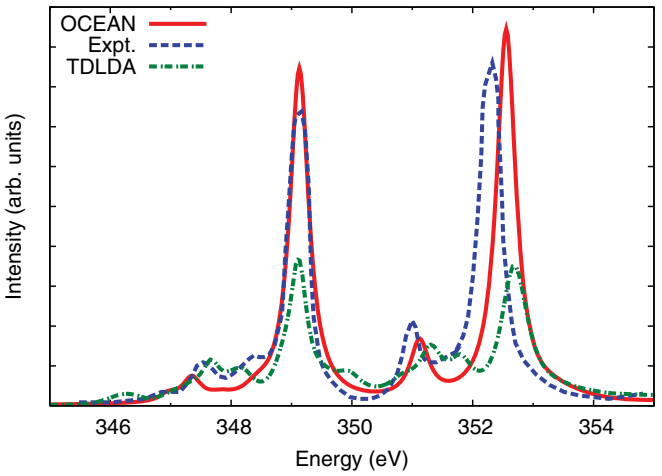

FIG. 2. (Color online) Calculated $L_{2,3}$ edge of Ca in CaF_2 using the BSE and TDLDA.[16] Note that the BSE yields a more accurate treatment of the peak intensity at both edges.

B. V and VO_2

Above the metal-insulator transition temperature, 340 K, VO_2 is a conductor with a rutile structure, but below this temperature the V atoms dimerize and the material becomes a monoclinic insulator. Both LDA and single-shot GW calculations incorrectly describe the low-temperature phase as a conductor. The failure of non-self-consistent GW to open a gap has been attributed to the inappropriateness of LDA wave functions to describe excited states. However, self-consistent GW (SCGW) leads to significant mixing of the initial wave functions around the Fermi level, e.g., the V d states which are probed in L-edge XANES. Following the method of Ref. 26, we first carried out self-consistent calculations within the COHSEX (Coulomb-hole/screened exchange) approximation to reduce computational time, and then a full frequency-dependent calculation, such that we numerically evaluated the frequency integral implicit in $\Sigma = iGW$. The screening was calculated within the RPA for a set of 5 imaginary and 60 real energy points selected utilizing a tangent function spacing determined by setting the midpoint to 30 eV and the maximum to 200 eV. The wave functions and self-energy corrections were calculated on a $4 \times 4 \times 4$ unshifted k-point grid.

As seen in Fig. 3, agreement with experiment is mostly unaffected by this SCGW calculation, despite the opening of an $\approx$1 eV band gap. This may be due in part to the local nature of core-level excitations. One possible source of error in our implementation is the spherical screening used in calculating the direct term, averaging the valence electron response between the two symmetry-split sets of unoccupied

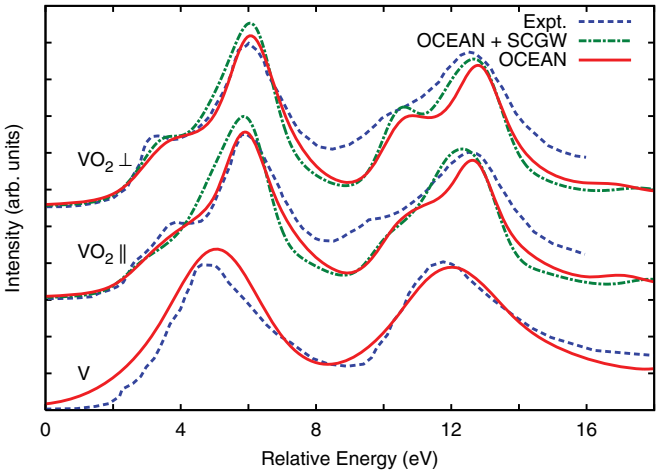

FIG. 3. (Color online) Calculated $L_{2,3}$ edges of metallic V[27] and M1 VO_2,[28] compared with experiment. The alignment of the metallic and insulating compounds was chosen to match at the L_3 edge. The VO_2 spectra are polarization dependent, shown with respect to the c axis of the rutile phase. BSE calculations were done using wave functions and energies from both the LDA (red, solid line) and self-consistent GW (green, dashed line).

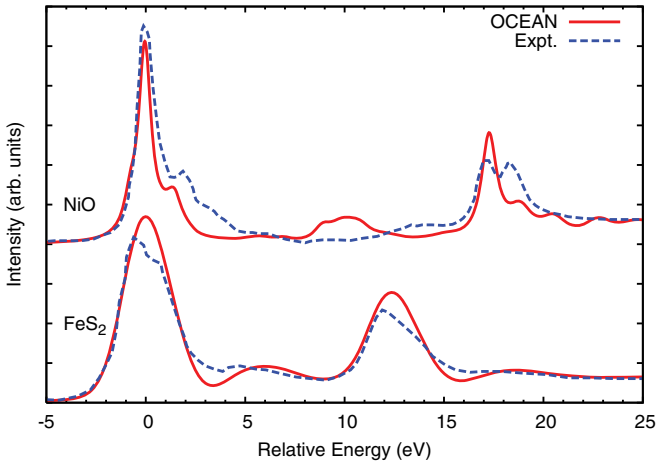

FIG. 4. (Color online) Calculated $L_{2,3}$ XANES of (top) NiO[29] and (bottom) FeS_2[30] compared to experiment. The calculation of the Ni $L_{2,3}$ edge in NiO is not in agreement with experiment, failing to reproduce the features 2 eV above both edges. While the L_3/L_2 ratio of FeS_2 is well reproduced, the splitting of the d bands is underestimated and the feature at 5 eV (and echoed at 13 eV) is slightly high in energy.

d states. While the SO splitting between the L_2 and L_3 edges agrees well with experiment and the edge ratio is significantly reduced, the ratio is still about 10% too high for both metallic vanadium and VO_2.

C. FeS_2 and NiO

As an illustration of calculations for heavier transition-metal insulators we compare iron pyrite FeS_2 with nickel oxide NiO. FeS_2 has a low-spin ground state, and unlike many other ionic, transition-metal compounds (halides, chalcogenides, or dichalcogenides) the ground-state electronic structure is described fairly well by the LDA. The agreement between the BSE in OCEAN and XAS experiment is excellent (Fig. 4). However, the calculation for FeS_2 slightly underestimates the spread of the unoccupied iron d states, and, more noticeably, the position of the 4s peak at 5 eV above the edge is slightly too high. This discrepancy could arise either from an incorrect ground-state band structure pushing the unoccupied 4s up in energy or from an overlocalization of the d states resulting in an overbinding of the corresponding exciton.

Nickel oxide (NiO) has an antiferromagnetic ground state and is treated here with an undistorted rocksalt structure. Unlike pyrite, nickel oxide is not well described using DFT. Consequently we carried out GW self-energy calculations for NiO within the self-consistent COHSEX approximation on top of an LSDA ground state which was sufficient to open a gap in the ground state. Frequency-dependent GW calculations might correct the relative spacing between the L_3 white line and the higher-energy fine structure, around 10 eV past the edge in our calculation, but have not been carried out here. At both the L_3 and L_2 edges the experiment shows a doubled structure, indicative of a charge-transfer excitation which is absent in the theoretical spectrum. Our current approach does not allow for localized, satellite excitations, and hence it cannot reproduce such features. In contrast, charge-transfer multiplet-based calculations explicitly allow for such features and yield results in significantly closer agreement with experiment for NiO.[3,5]

D. Fe, Co, and Ni metals

The group-VIII metals all have L_3/L_2 ratios of 2.0 or higher, and their spectra are dominated by white lines. Our approach for calculating these metals is currently limited by the use of LSDA wave functions, a spin agnostic self-energy, and static screening. However, dynamical mean-field theory (DMFT) calculations of the densities of states (DOS) for these metals exhibit a large spin dependence in the self-energy and a shift of the minority-spin DOS toward the Fermi level.[31] Such a shift would improve the agreement in the near-edge region [Fig. 5(a)] of both Fe and Co, where the unoccupied LSDA states peak too high above the Fermi level. Moreover, our GW BSE calculations systematically overestimate the relative strength of the L_2 peak by about 10–20%, and there is a clear asymmetry in the white lines, characteristic of a Fano line shape. Going beyond the GW approximation and expressing the quasiparticle self-energy as a cumulant expansion, the strength of the asymmetry can be identified with the slope of the quasiparticle lifetime.[32] Here, the electron-hole pair dependence of the asymmetry is neglected, and a constant asymmetry of 5% is applied via convolution to the group-VIII metals. Finally we attribute the underestimation of spectral weight around 6 eV above the white lines to satellite excitations not accounted for in the BSE approach. In contrast, the feature at 7 eV in Ni (higher in Co and Fe) appears in calculations neglecting electron-hole interactions (not shown) and has been attributed to a band-structure effect.[33]

E. Cu

Copper, with its filled d band, lacks the characteristic white lines that dominate the spectra of all lighter transition

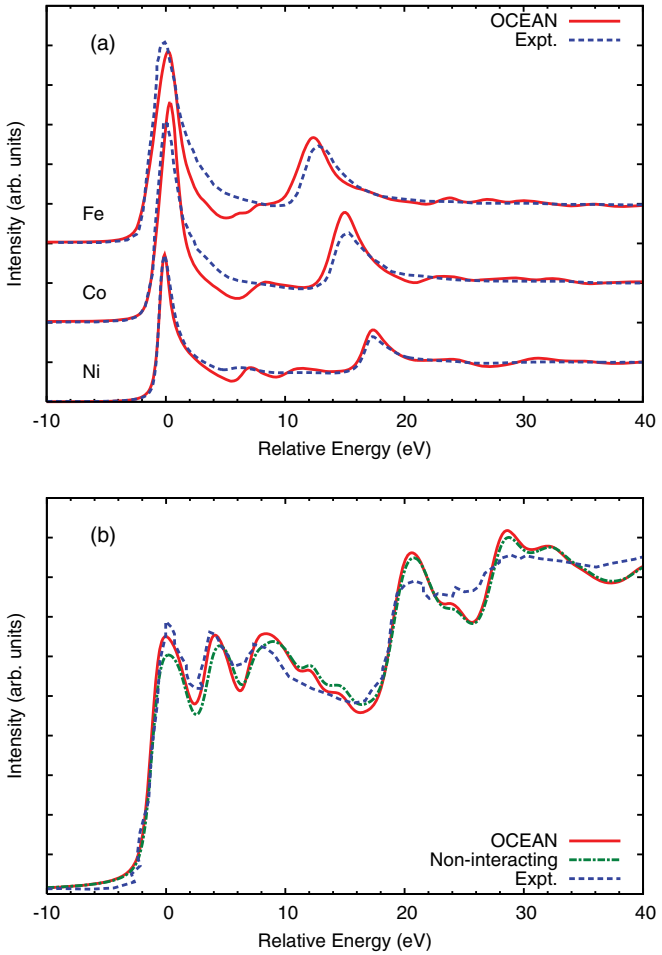

FIG. 5. (Color online) Calculations of the $L_{2,3}$ edge XAS of (a) metallic Fe, Co, and Ni compared with experiment[35,36] and (b) metallic Cu with (OCEAN) and without (noninteracting) electron-hole interaction terms.[37] The group-VIII metals are normalized to the high-energy tails and all the spectra are aligned at the L_3 edge to show the evolution of the SO splitting.

metals. Taking advantage of the lack of unoccupied d states and efficient core-hole screening, ground-state calculations ignoring both excitonic and multiplet effects were shown to give reasonable results for the copper $L_{2,3}$ edge.[34] However, our GW BSE approach clearly gives improved agreement with experiment at the edge, where the core-hole potential is not completely screened, and also accounts for the excitonic enhancement of the edge [Fig. 5(b)]. The multipole components of the exchange and direct term in copper are small and have similar magnitudes, leading to cancellation.

IV. CONCLUSIONS

In summary, we have developed a MBPT GW BSE approach for calculations of core-level L-shell spectra that to a good approximation unifies extended-state and atomic multiplet approaches. Overall the approach developed here clearly shows the power of the GW BSE method implemented in OCEAN and does a near quantitative job of reproducing the core-level $L_{2,3}$-edge XANES of 3d transition-metal materials, as summarized in Table I. The ratios have been estimated to within ± 0.1 from the heights of the L_3 and L_2 peaks, as in Ref. 38. However, several limitations of our current GW BSE implementation currently exist, in particular, the reliance on DFT for the ground state and the neglect of dynamic effects in the screening and satellites in the spectra. With the exceptions of VO_2 and NiO, the ground states of all systems studied are well characterized by the L(S)DA. This was primarily a matter of convenience since (as for VO_2) self-consistent GW calculations can be used to correct some shortcomings in the DFT. Alternative methods for correcting DFT calculations of transition-metals include DMFT[31] and Hubbard model corrections.[39,40]

TABLE I. L_3/L_2 peak ratio vs Z.

Atom	Z	Expt.[38]	OCEAN	Atom	Z	Expt.	OCEAN
Ca	20	0.8	0.8	Co	27	2.3	2.0
V	23	1.0	1.1	Ni	28	2.4	2.0
Fe	26	2.0	1.8	Cu	29	0.9	0.8

Several of these limitations can be addressed by extensions of our approach which are relegated to the future. In particular it is desirable to go beyond the quasiparticle electron-hole framework of the BSE, including coupling to excitations such as phonons and multielectron processes which give rise to satellites in the spectra. Such satellite excitations are likely responsible for the missing weight at about 6 eV above the edge in the group-VIII metals [Fig. 5(a)]. The inclusion of secondary excitations, such as charge-transfer and d-d^* excitations in transition-metal oxides, is important for quantitative agreement with experiment and has been included explicitly in charge-transfer multiplet calculations.[4,5] Adding these terms to the GW BSE approach can be accomplished using a core-level spectral function[41] and coupling to a local Hamiltonian similar to that in charge-transfer multiplet calculations[2] or an explicit extension of H_{BSE} to include interactions with secondary particle-hole pairs. Also, the inclusion of dynamic screening, e.g., coupling to plasmonic excitations in W, should be investigated, especially in transition-metal systems when the plasmon energy is comparable to the spin-orbit splitting.

ACKNOWLEDGMENTS

This work was supported by Department of Energy (DOE) BES Grant No. DE-FG03-97ER45623 and facilitated by the DOE Computational Materials Science Network. We thank H. Ebert, F. M. F. de Groot, H. Ikeno, K. Jorissen, P. Kruger, L. Reining, E. L. Shirley, and especially J. J. Kas for useful comments and discussions.

[1] R. D. Leapman and L. A. Grunes, Phys. Rev. Lett. **45**, 397 (1980).
[2] F. M. F. de Groot, Coordination Chemistry Reviews **249**, 31 (2005).
[3] M. W. Haverkort, M. Zwierzycki, and O. K. Andersen, Phys. Rev. B **85**, 165113 (2012).

[4]P. S. Miedema, H. Ikeno, and F. M. F. de Groot, J. Phys.: Condens. Matter **23**, 145501 (2011).
[5]H. Ikeno, T. Mizoguchi, and I. Tanaka, Phys. Rev. B **83**, 155107 (2011).
[6]A. L. Ankudinov, Y. Takimoto, and J. J. Rehr, Phys. Rev. B **71**, 165110 (2005).
[7]A. L. Ankudinov, A. I. Nesvizhskii, and J. J. Rehr, Phys. Rev. B **67**, 115120 (2003).
[8]O. Bunău and Y. Joly, Phys. Rev. B **85**, 155121 (2012).
[9]P. Krüger and C. R. Natoli, Phys. Rev. B **70**, 245120 (2004).
[10]P. Krüger, Phys. Rev. B **81**, 125121 (2010).
[11]R. Laskowski and P. Blaha, Phys. Rev. B **82**, 205104 (2010).
[12]E. L. Shirley, Ultramicroscopy **106**, 986 (2006).
[13]J. Vinson, J. J. Rehr, J. J. Kas, and E. L. Shirley, Phys. Rev. B **83**, 115106 (2011).
[14]X. Gonze *et al.*, Comput. Phys. Commun. **180**, 2582 (2009).
[15]X. Gonze *et al.*, Zeit. Kristallogr. **220**, 558 (2005).
[16] E. L. Shirley, J. Electron Spectrosc. Relat. Phenom. **144–147**, 1187 (2005).
[17]J. Vinson, J. J. Kas, F. D. Vila, J. J. Rehr, and E. L. Shirley, Phys. Rev. B **85**, 045101 (2012).
[18]J. J. Kas, A. P. Sorini, M. P. Prange, L. W. Cambell, J. A. Soininen, and J. J. Rehr, Phys. Rev. B **76**, 195116 (2007).
[19]H. M. Lawler, J. J. Rehr, F. Vila, S. D. Dalosto, E. L. Shirley, and Z. H. Levine, Phys. Rev. B **78**, 205108 (2008).
[20]P. E. Blöchl, Phys. Rev. B **50**, 17953 (1994).
[21]J. A. Soininen and E. L. Shirley, Phys. Rev. B **64**, 165112 (2001).
[22]See http://opium.sourceforge.net.
[23]E. Luppi, H.-C. Weissker, S. Bottaro, F. Sottile, V. Veniard, L. Reining, and G. Onida, Phys. Rev. B **78**, 245124 (2008).
[24]K. Gilmore and E. L. Shirley, J. Phys.: Condens. Matter **22**, 315901 (2010).
[25]J. Fink, T. Müller-Heinzerling, B. Scheerer, W. Speier, F. U. Hillebrecht, J. C. Fuggle, J. Zaanen, and G. A. Sawatzky, Phys. Rev. B **32**, 4899 (1985).
[26]M. Gatti, F. Bruneval, V. Olevano, and L. Reining, Phys. Rev. Lett. **99**, 266402 (2007).
[27]A. Scherz, Ph.D. thesis, Freie Universität, Berlin, 2003.
[28]M. W. Haverkort *et al.*, Phys. Rev. Lett. **95**, 196404 (2005).
[29]G. van der Laan, J. Zaanen, G. A. Sawatzky, R. Karnatak, and J.-M. Esteva, Phys. Rev. B **33**, 4253 (1986).
[30]K. C. Prince, M. Matteucci, K. Kuepper, S. G. Chiuzbaian, S. Bartkowski, and M. Neumann, Phys. Rev. B **71**, 085102 (2005).
[31]A. Grechnev, I. Di Marco, M. I. Katsnelson, A. I. Lichtenstein, J. Wills, and O. Eriksson, Phys. Rev. B **76**, 035107 (2007).
[32]F. Aryasetiawan, L. Hedin, and K. Karlsson, Phys. Rev. Lett. **77**, 2268 (1996).
[33]A. I. Nesvizhskii, A. L. Ankudinov, J. J. Rehr, and K. Baberschke, Phys. Rev. B **62**, 15295 (2000).
[34]B. I. Cho *et al.*, Phys. Rev. Lett. **106**, 167601 (2011).
[35]C. T. Chen, Y. U. Idzerda, H.-J. Lin, N. V. Smith, G. Meigs, E. Chaban, G. H. Ho, E. Pellegrin, and F. Sette, Phys. Rev. Lett. **75**, 152 (1995).
[36]C. T. Chen, N. V. Smith, and F. Sette, Phys. Rev. B **43**, 6785 (1991).
[37]S. Kiyono, S. Chiba, Y. Hayasi, S. Kato, and S. Mochimaru, Jpn. J. Appl. Phys. **17S2**, 212 (1978).
[38]J. Schwitalla and H. Ebert, Phys. Rev. Lett. **80**, 4586 (1998).
[39]T. Miyake and F. Aryasetiawan, Phys. Rev. B **77**, 085122 (2008).
[40]T. Ahmed, J. J. Kas, and J. J. Rehr, Phys. Rev. B **85**, 165123 (2012).
[41]L. Hedin, J. Phys.: Condens. Matter **11**, R489 (1999).